Electronic Supplementary Material (ESI) for Nanoscale
This journal is © The Royal Society of Chemistry 2024

Supplementary Information

Bi-doped Ruthenium Oxide Nanocrystal for Water Oxidation in Acidic Media

Shiyao Chen[a], Hai Liu[a], Bichen Yuan[a], Wenhai Xu[a], Aiqing Cao[a], Marshet Getaye Sendeku[b], Yaping Li[a,*], Xiaoming Sun[a,*], Fengmei Wang[a,*]

a. *State Key Laboratory of Chemical Resource Engineering, College of Chemistry, Beijing University of Chemical Technology, Beijing 100029, P. R. China.*

b. *Ocean Hydrogen Energy R&D Center, Research Institute of Tsinghua University in Shenzhen, Shenzhen, P. R. China.*

**E-mail: wangfm@buct.edu.cn; sunxm@mail.buct.edu.cn; liyp@mail.buct.edu.cn*

Supplementary Note 1

The Gibbs free energy of absorbed species (G_{*ads}) can be computed using following equation[1]:

$$G_{*ads} = E + ZPE - TS$$

In this equation, **ads* represents the adsorbed species, such as *OH, *O, *OOH, or *H. The term *G* represents the Gibbs free energy of the adsorbed species, while *E* refers to the energy obtained from Density Functional Theory (DFT) calculation, *ZPE* stands for zero-point energy, *S* represents entropy and *T* denotes the temperature, which was set at 298.15 K for this study.

The oxygen evolution reaction (OER) under acidic conditions, a four-electron transfer process, comprises four distinct reaction steps (Figure 4a, 4b). Both AEM and LOM mechanisms share the common initial stages, which are evaluated using Equations 1 and 2. Subsequently, AEM proceeds with the next two stages, calculated by Equations 3 and 4 (Figure 4a),[2] whereas LOM continues with Equations 5 and 6 (Figure 4b).[3] The Gibbs free energy of ($H^+ + e^-$) at standard conditions is assumed as the free energy of 1/2 H_2.

$$H_2O + * \leftrightarrow HO^* + H^+ + e^- \quad \text{(equation 1)}$$

$$\Delta G_1 = \Delta G_{HO^*} + 1/2\Delta G_{H_2} - \Delta G_* - \Delta G_{H_2O} - eU$$

$$HO^* \leftrightarrow O^* + H^+ + e^- \quad \text{(equation 2)}$$

$$\Delta G_2 = \Delta G_{O^*} + 1/2\Delta G_{H_2} - \Delta G_{HO^*} - eU$$

$$O^* + H_2O \leftrightarrow HOO^* + H^+ + e^- \quad \text{(equation 3)}$$

$$\Delta G_3 = \Delta G_{HOO^*} + 1/2\Delta G_{H_2} - \Delta G_{O^*} - \Delta G_{H_2O} - eU$$

$$HOO^* \leftrightarrow \square^* + O_2 + H^+ + e^- \quad \text{(equation 4)}$$

$$\Delta G_4 = \Delta G_* + 1/2\Delta G_{H_2} + \Delta G_{O_2} - \Delta G_{HOO^*} - eU$$

$$O^* + H_2O \leftrightarrow H^* + H^+ + e^- + O_2 \quad \text{(equation 5)}$$

$$\Delta G_3' = \Delta G_{H^*} + 1/2\Delta G_{H_2} + \Delta G_{O_2} - \Delta G_{O^*} - \Delta G_{H_2O} - eU$$

$$H^* \leftrightarrow \square^* + H^+ + e^- \quad \text{(equation 6)}$$

$$\Delta G_4' = \Delta G_* + 1/2\Delta G_{H_2} - \Delta G_{H^*} - eU$$

In this work, $\Delta G_{1\text{-}4}^{(\prime)}$ values were calculated at $U = 0$ V.

Supplementary Note 2

To clarify the effect of varying loadings on the activity of the $Bi_{0.05}Ru_{0.95}O_2$ catalyst, the Turnover Frequency (TOF) value was calculated.

$$\text{TOF} = \frac{J*A}{4*e*n}$$

J is current density obtained at 1.5 V (vs. RHE) and normalized by geometric area; *A* is the geometric area; e is the charge of electron ($1.602 * 10^{-19}$ C) and *n* is the number of active sites, calculated *via* the following equation.

This method is calculating based on all Ru atoms, from the following equation:

$$n = \frac{m_{loading} * N_A}{M_W} * n_{metal}$$

where $m_{loading}$ is the loading mass of catalyst on carbon paper, n_{metal} is the mole number of metal atoms such as Ru per mole of electrocatalysts and M_w is the molecular weight of catalyst.

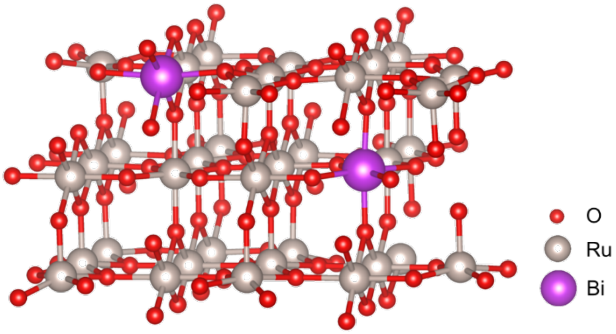

Figure S1 Slab model of $Bi_2Ru_{34}O_{72}$ after structural optimization.

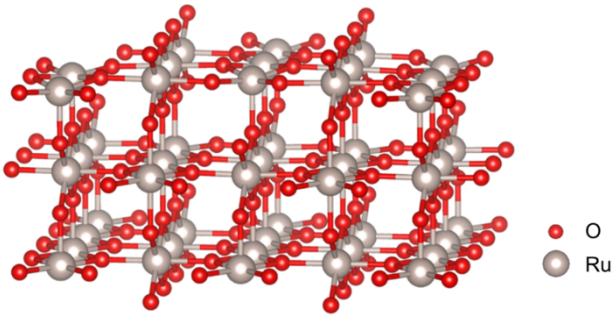

Figure S2 Slab model of RuO_2 after structural optimization.

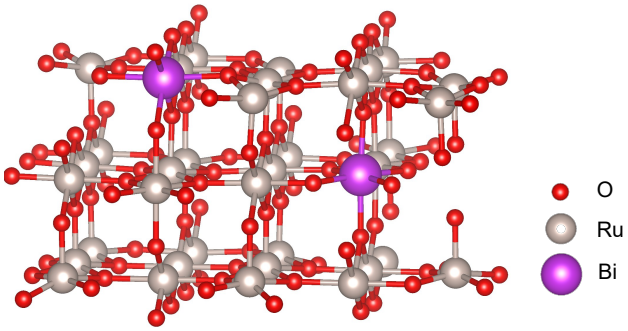

Figure S3 Slab model of Bi-O_v-RuO_2 after structural optimization.

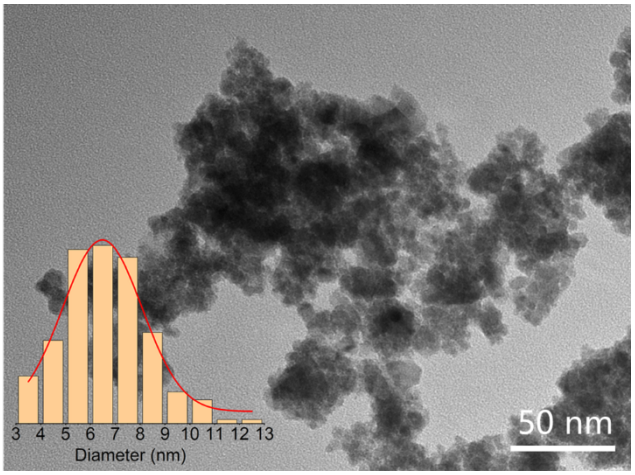

Figure S4 TEM image of $Bi_{0.05}Ru_{0.95}O_2$, inset showing particle size distribution.

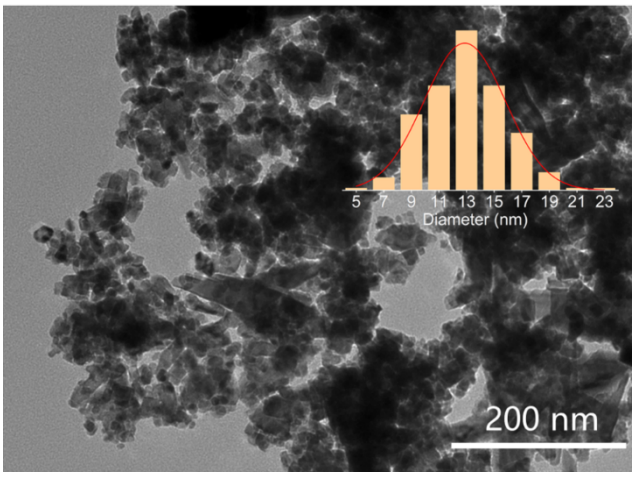

Figure S5 TEM image of HM-RuO_2, inset showing particle size distribution.

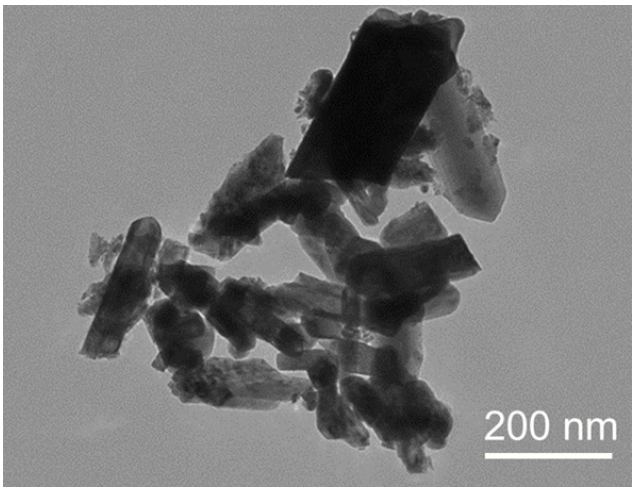

Figure S6 TEM image of C-RuO_2.

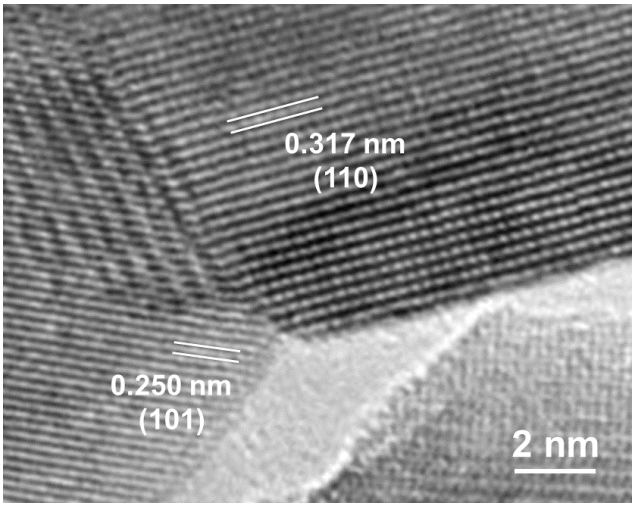

Figure S7 HRTEM image of C-RuO_2.

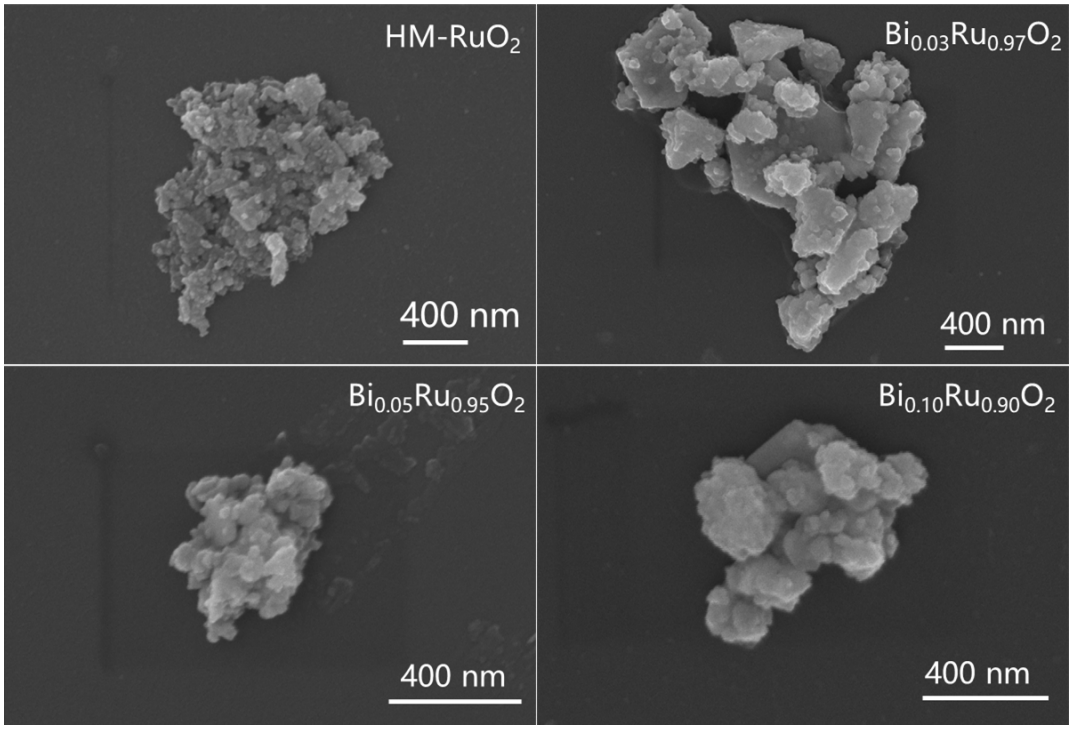

Figure S8 SEM images of HM-RuO_2, $Bi_{0.03}Ru_{0.97}O_2$, $Bi_{0.05}Ru_{0.95}O_2$, $Bi_{0.10}Ru_{0.90}O_2$.

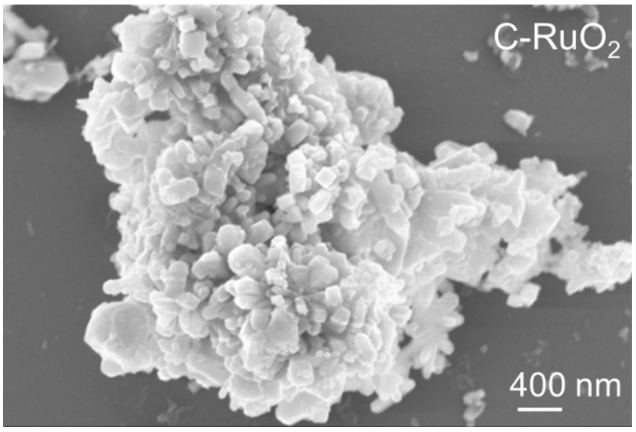

Figure S9 SEM image of C-RuO_2.

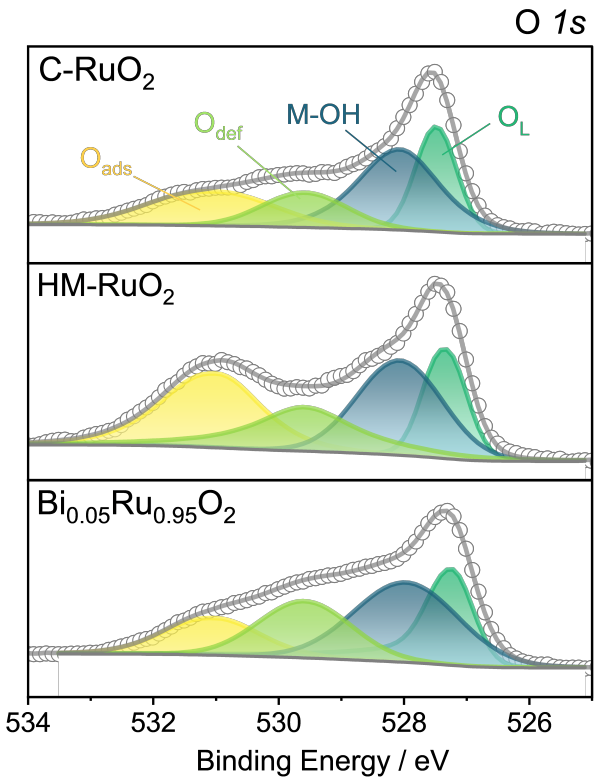

Figure S10 O *1s* XPS spectra of $Bi_{0.05}Ru_{0.95}O_2$, HM-RuO_2 and C-RuO_2. More details are shown in Table S2.

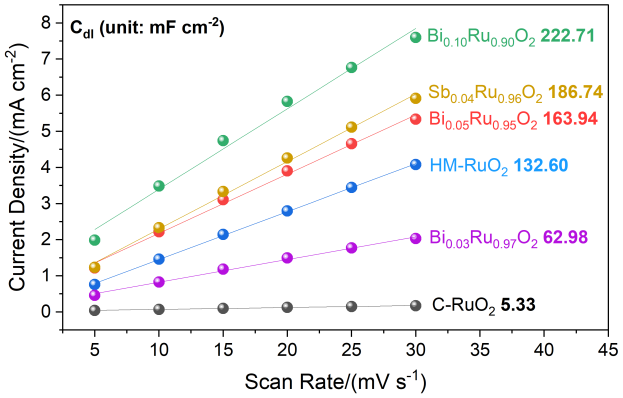

Figure S11 C_{dl} linear fitting plot of $Bi_xRu_{1-x}O_2$, $Sb_{0.04}Ru_{0.96}O_2$, HM-RuO_2 and C-RuO_2 derived from CV curves.

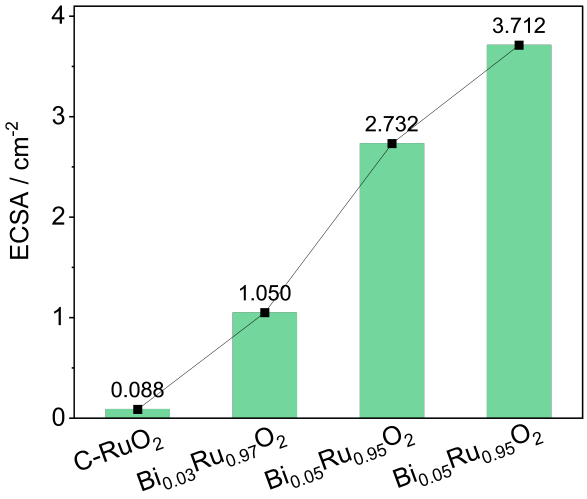

Figure S12 Comparison of electrochemical active surface areas of $Bi_xRu_{1-x}O_2$ and C-RuO_2.

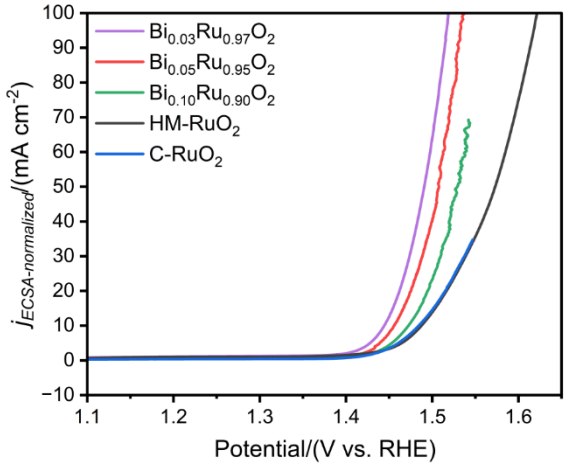

Figure S13 Specific activity curves of $Bi_xRu_{1-x}O_2$, HM-RuO_2 and C-RuO_2 electrode collected at the scan rate of 5 mV s^{-1} in 0.5 M H_2SO_4 electrolyte.

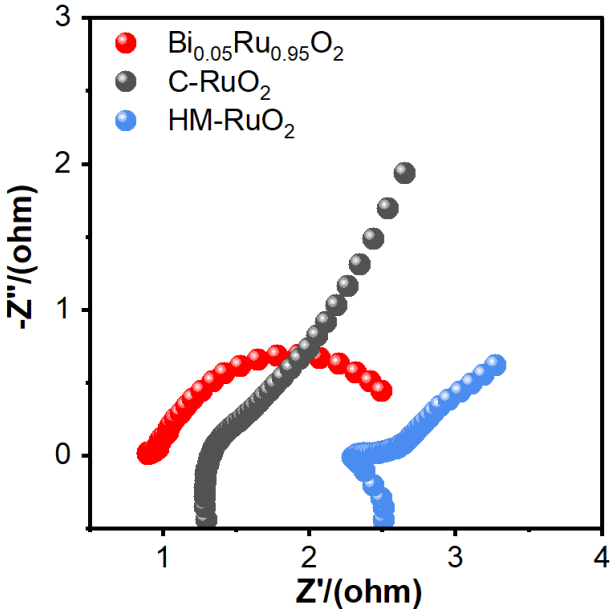

Figure S14 EIS plot of $Bi_{0.05}Ru_{0.95}O_2$, HM-RuO_2 and C-RuO_2 at a voltage (init E) of 1.24 V in 0.5 M H_2SO_4 electrolyte. The frequency range for testing is from 100 kHz to 1 Hz.

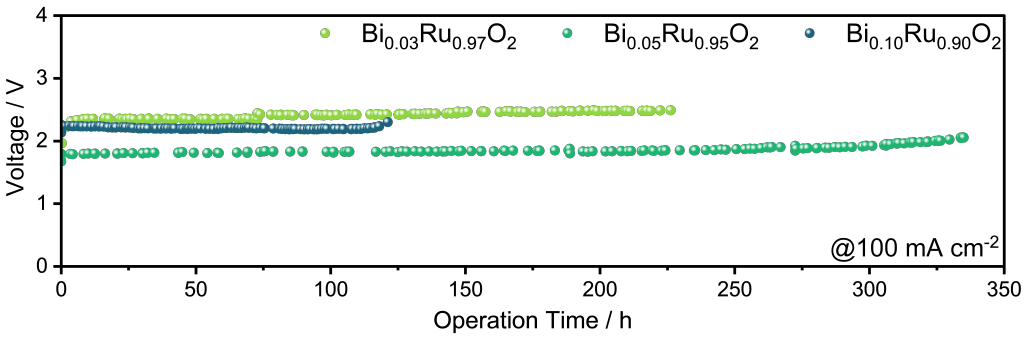

Figure S15 Chronopotentiometry tests of $Bi_xRu_{1-x}O_2$ at 100 mA cm^{-2} in 0.5 M H_2SO_4 electrolyte.

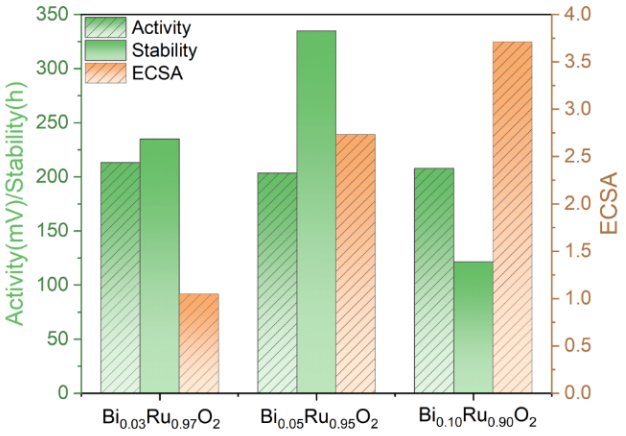

Figure S16 Comparison of activity (overpotential@10 mA cm^{-2}) and stability (at 100 mA cm^{-2}) among various $Bi_xRu_{1-x}O_2$.

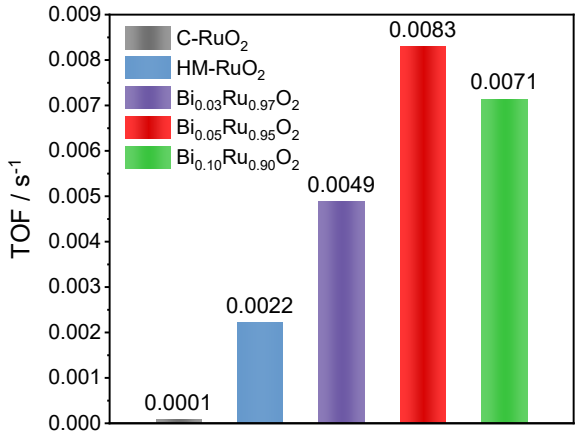

Figure S17 Turnover frequency comparison of $Bi_xRu_{1-x}O_2$, HM-RuO_2 and C-RuO_2.

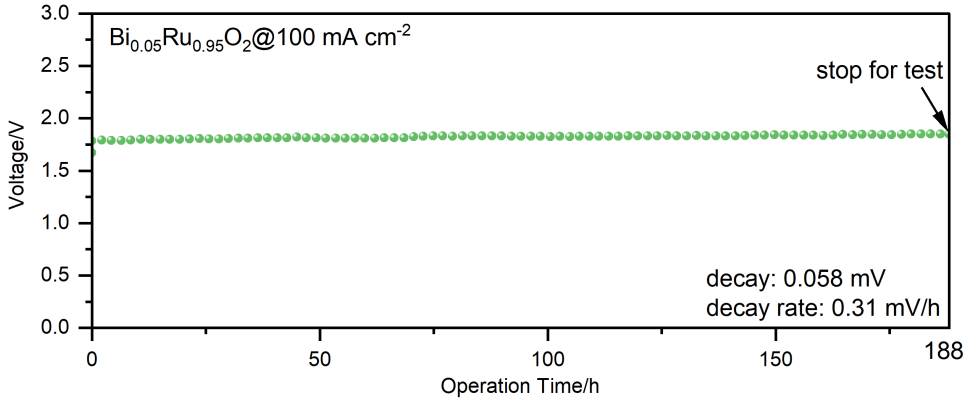

Figure S18 Chronopotentiometry test of $Bi_{0.05}Ru_{0.95}O_2$ in 0.5 M H_2SO_4 electrolyte at 100 mA cm^{-2} for 188 h. The electrode after the stability test was used for subsequent tests.

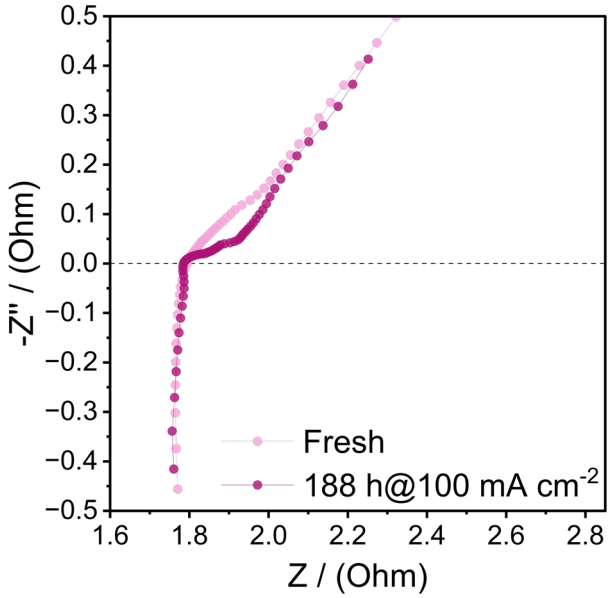

Figure S19 EIS plots of $Bi_{0.05}Ru_{0.95}O_2$ at a voltage (init E) of 1.24 V in 0.5 M H_2SO_4 electrolyte before and after 188-h stability test at 100mA cm^{-2}. The frequency range for testing is from 100 kHz to 1 Hz.

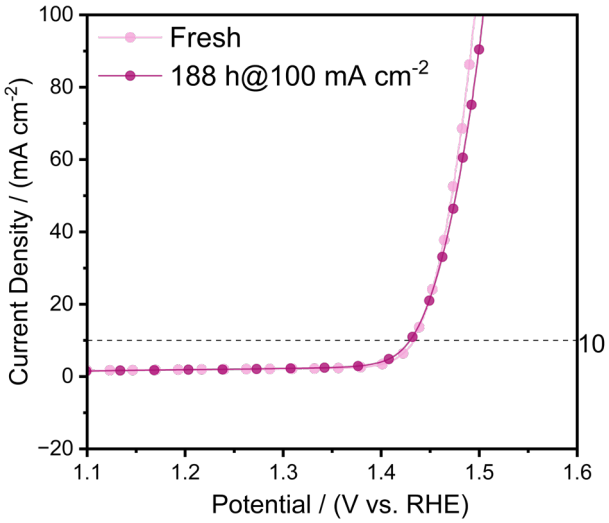

Figure S20 Polarization curves at the scan rate of 5 mV s^{-1} for $Bi_{0.05}Ru_{0.95}O_2$ electrode in 0.5 M H_2SO_4 electrolyte before and after 188-h stability test at 100mA cm^{-2}.

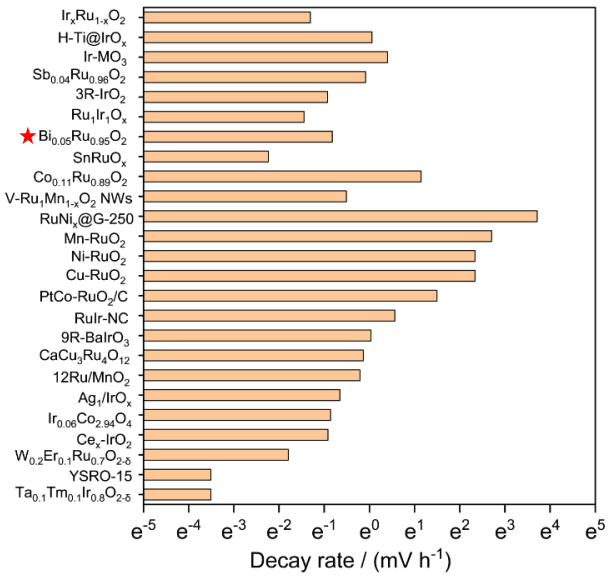

Figure S21 Comparison of decay rate (mV h^{-1}) between $Bi_{0.05}Ru_{0.95}O_2$, $Sb_{0.04}Ru_{0.96}O_2$ and recently-reported Ru- and Ir-based catalysts.

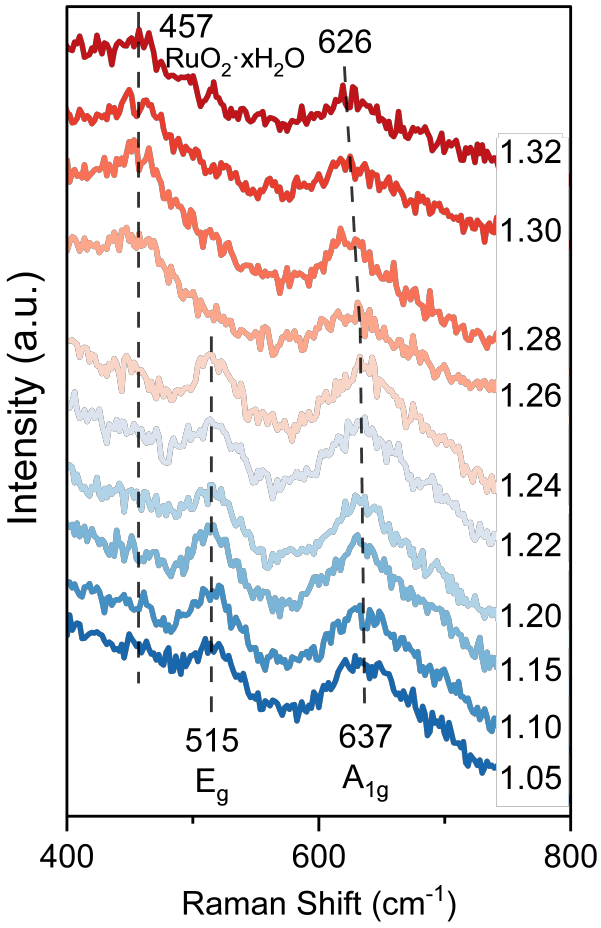

Figure S22. In-situ Raman spectra collected form $Bi_{0.05}Ru_{0.95}O_2$ catalyst in 0.1 M $HClO_4$.

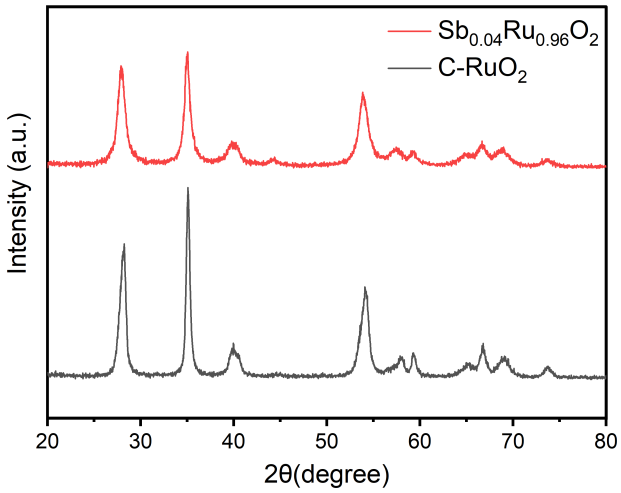

Figure S23 XRD patterns of $Sb_{0.04}Ru_{0.96}O_2$ and C-RuO_2.

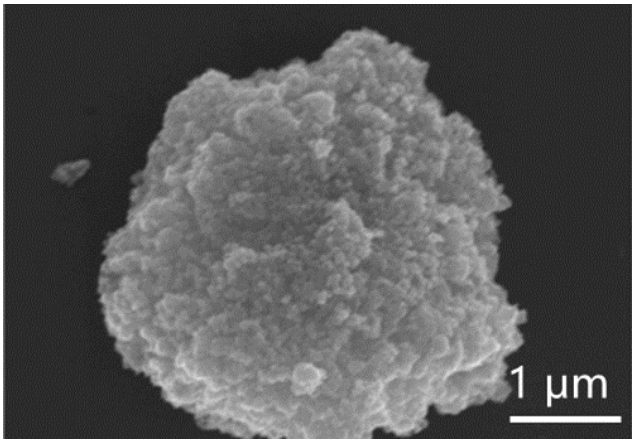

Figure S24 SEM image of $Sb_{0.04}Ru_{0.96}O_2$.

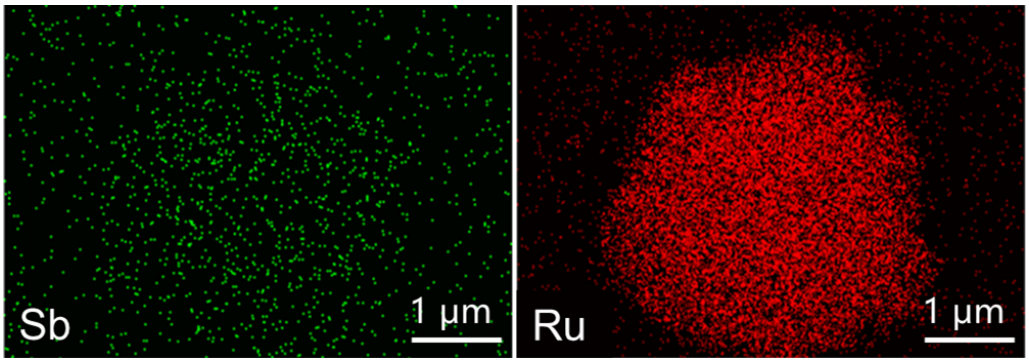

Figure S25 Element mapping of $Sb_{0.04}Ru_{0.96}O_2$.

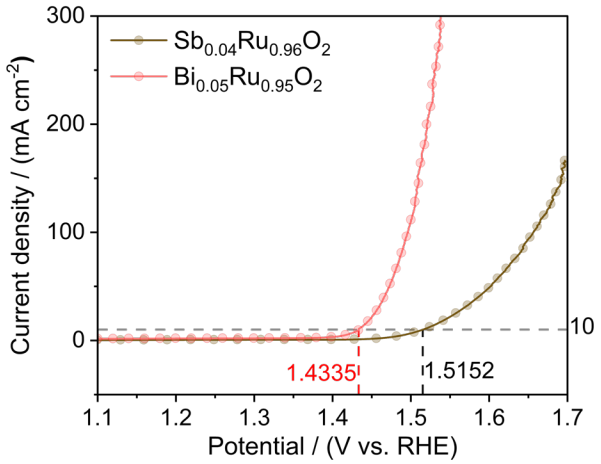

Figure S26 Polarization curves at the scan rate of 5 mV s^{-1} for $Sb_{0.04}Ru_{0.96}O_2$ and $Bi_{0.05}Ru_{0.95}O_2$ electrodes in 0.5 M H_2SO_4 electrolyte.

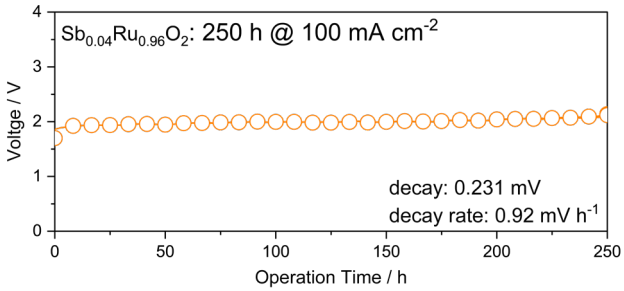

Figure S27 Stability test of $Sb_{0.04}Ru_{0.96}O_2$ electrode at the current density of 100 mA cm^{-2} in 0.5 M H_2SO_4.

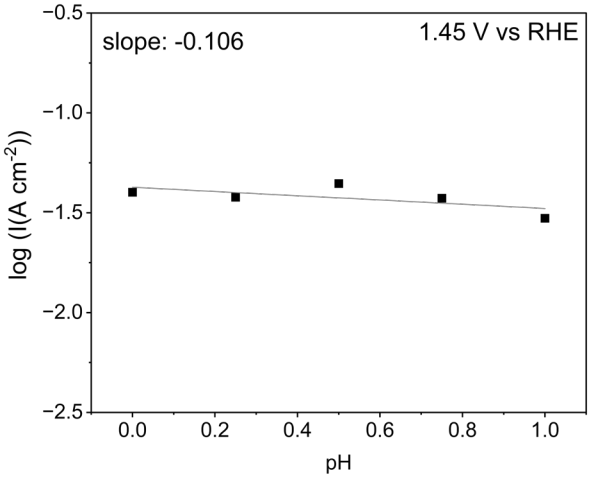

Figure S28 Log (I (A cm^{-2})) of $Bi_{0.05}Ru_{0.95}O_2$ electrode at 1.45 V vs. RHE as a function of pH.

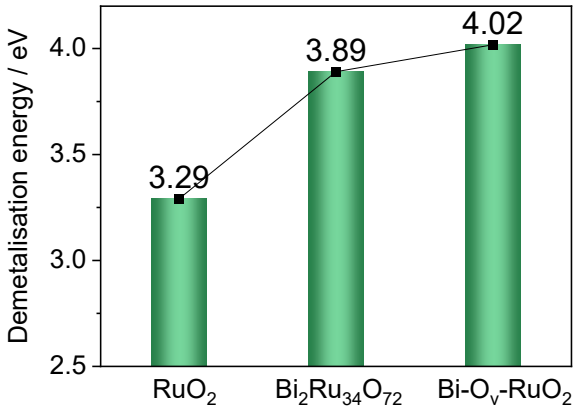

Figure S29 The demetalisation energies of RuO_2, $Bi_2Ru_{34}O_{72}$ and Bi-O_v-RuO_2.

Table S1 The atomic ratio of Ru and Bi collected from EDS analysis of various $Bi_xRu_{1-x}O_2$ samples.

Sample	Element	Atomic ratio [%]
$Bi_{0.03}Ru_{0.97}O_2$	Bi	2.50
	Ru	97.50
$Bi_{0.05}Ru_{0.95}O_2$	Bi	4.82
	Ru	95.18
$Bi_{0.10}Ru_{0.90}O_2$	Bi	9.90
	Ru	90.10

Table S2 Fitting results of the O l*s* XPS spectra for $Bi_{0.05}Ru_{0.95}O_2$, HM-RuO_2 and C-RuO_2 (after carbon-correction).

Samples	O_L		M-OH		O_V		O_{ads}	
	Position /eV	Area (ratio)	Position /eV	Area (ratio)	Position /eV	Area (ratio)	Position /eV	Area (ratio)
C-RuO_2	527.48	24156 (23.6%)	528.06	38244 (37.4%)	529.58	16210 (15.8%)	531.01	23742 (23.2%)
HM-RuO_2	527.33	17551 (18.4%)	528.06	29686 (31.1%)	529.58	19745 (20.7%)	530.98	28473 (29.8%)
$Bi_{0.05}Ru_{0.95}O_2$	527.24	27824 (24.4%)	527.96	41922 (36.8%)	529.58	26244 (23.0%)	531.01	17996 (15.8%)

Table S3 Overpotential values collected from various $Bi_xRu_{1-x}O_2$ electrode at 10 mA cm^{-2}.

Samples	Overpotential/mV
HM-RuO_2	227.8
$Bi_{0.03}Ru_{0.97}O_2$	213.2
$Bi_{0.05}Ru_{0.95}O_2$	**203.5**
$Bi_{0.10}Ru_{0.90}O_2$	207.8
C-RuO_2	403.0

Table S4 Comparison of C_{dl} values and the relative ratio to demonstrate the ECSA changes of various electrocatalysts.

Catalysts	C_{dl} / [mF cm^{-2})]	C_{dl} /C_s
$Bi_{0.03}Ru_{0.97}O_2$	62.98	1.05
$Bi_{0.05}Ru_{0.95}O_2$	**163.94**	**2.73**
$Bi_{0.10}Ru_{0.90}O_2$	222.71	3.71
$Sb_{0.04}Ru_{0.96}O_2$	186.74	3.11
C-RuO_2	5.33	0.09
HM-RuO_2	132.60	2.21

Table S5 The comparison of Tafel slope, overpotential and durability test performance of $Bi_{0.05}Ru_{0.95}O_2$ and HM-RuO_2 with recently reported electrocatalysts in 0.5 M H_2SO_4.

Catalyst	Tafel slope / (mV dec^{-1})	Overpotential / (mV)	Reference
$Bi_{0.05}Ru_{0.95}O_2$	**52.90**	**203.5**	**This work**
HM-RuO_2	**71.64**	**227.8**	**This work**
$Ru_{0.6}Cr_{0.2}Ti_{0.2}O_2$	58	267	*J Am Chem Soc*, 2024, **146**, 15740-15750[4]
$Ru_1Ir_1O_x$	71.3	204	*Advanced Energy Materials*, 2021, **11,** 2102883[5]
Ru-UiO-bpydc	78.3	200	*Chem*, 2023, **9**, 1882-1896[6]
$(Ru, Mn)_2O_3$	68.7	168	*Nano Energy*, 2023, **115**, 108727[7]
SA Zn-RuO_2	56	210	*Journal of Energy Chemistry*, 2024, **88**, 94-102[8]
$Ru_2(S_3Se)$	72	186	*Energy & Environmental Science*, 2024, **17**, 1885-1893[9]
CoO_x/RuO_x-CC	61.2	180	*Small*, 2023, **19**, e2302238[10]
9R-$BaIrO_3$	80	230	*J Am Chem Soc*, 2021, **143**, 18001-18009[11]

Table S6 The comparison of durability test performance of $Bi_{0.05}Ru_{0.95}O_2$ and $Sb_{0.04}Ru_{0.96}O_2$ with recently reported electrocatalysts in 0.5 M H_2SO_4.

catalyst	current density / (mA cm^{-2})	operation time / h	decay rate / (mV h^{-1})	reference
$Bi_{0.05}Ru_{0.95}O_2$	**100**	**>300**	**0.44**	**This work**
$Sb_{0.04}Ru_{0.96}O_2$	**100**	**250**	**0.92**	**This work**
$Ru_{0.6}Cr_{0.2}Ti_{0.2}O_2$	100	200	0.025	*J Am Chem Soc*, 2024, **146**, 15740-15750[4]
$Ru_1Ir_1O_x$	100	110	0.236	*Advanced Energy Materials*, 2021, **11**, 2102883[5]
Ru-UiO-bpydc	50	140	0.894	*Chem*, 2023, **9**, 1882-1896.[6]
$(Ru, Mn)_2O_3$	10	40	5.06	*Nano Energy*, 2023, **115**, 108727[7]
SA Zn-RuO_2	10	43	4.32	*Journal of Energy Chemistry*, 2024, **88**, 94-102[8]
$Ru_2(S_3Se)$	10	50	Stable	*Energy & Environmental Science*, 2024, **17**, 1885-1893[9]
CoO_x/RuO_x-CC	10	60	0.786	*Small*, 2023, **19**, e2302238[10]
9R-$BaIrO_3$	10	48	1.04	*J Am Chem Soc*, 2021, **143,** 18001-18009[11]
$SnRuO_x$	100	250	0.107	*Nat Commun*, 2023, **14**, 843[12]
3R-IrO_2	100	42	0.396	*Joule*, 2021, **5**, 3221-3234[13]
Ir-MoO_3	100	48	1.496	*Nat Commun*, 2021, 12, 5676[14]
V-$Ru_xMn_{1-x}O_2$ NWs	50	101	0.6	*Journal of Materials Chemistry A*, 2023, **11**, 25252-25261[15]
Sm_3IrO_7	10	10	24.02	*ACS Applied Materials & Interfaces*, 2023, **15**, 14282-14290[16]
MD-RuO_2-BN	10	24	1.2	*Nat Commun*, 2024, **15,** 3928[17]
RuIr-NC	10	40	1.759	*Nat Commun*, 2021, **12**, 1145[18]

$Nd_{0.1}RuO_x$/CC	10	25	0.6	*Advanced Functional Materials*, 2023, **33**, DOI: 10.1002/adfm.202213304[19]
Y_2MnRuO_7	10	40	0.3	*Nat Commun*, 2023, **14**, 2010[20]
$Li_{0.52}RuO_2$	10	70	1.694	*Nat Commun*, 2022, **13**, 3784[21]
$RuCoO_x$	10	100	0.45	*J Am Chem Soc*, 2023, **145**, 17995-18006[22]
Mn-RuO_2-450	10	150	0.267	*Small*, 2024, **20**, e2400754[23]
RuO_{2-x}/$RuSe_2$	10	200	Stable	*Advanced Functional Materials*, 2024, DOI: 10.1002/adfm.202406587[24]
12Ru/MnO_2	10	200	0.815	*Nature Catalysis*, 2021, **4**, 1012-1023[25]
PtCo-RuO_2/C	10	20	4.47	*Energy & Environmental Science*, 2022, **15**, 1119-1130[26]
Ag_1/IrO_x	10	50	0.52	*ACS Energy Letters*, 2021, DOI: 10.1021/acsenergylett.1c00283, 1588-1595[27]
Ni-RuO_2	10	8	10.4	*Nat Mater*, 2023, **22**, 100-108[28]
$Ir_{0.06}Co_{2.94}O_4$	10	200	0.424	*J Am Chem Soc*, 2021, **143**, 5201-5211[29]

Table S7 The atomic ratio of Ru and Sb collected from EDS analysis of $Sb_{0.04}Ru_{0.96}O_2$ sample.

Sample	Element	Atomic ratio [%]
$Sb_{0.04}Ru_{0.96}O_2$	Sb	4.14
	Ru	95.86

Table S8 Relative Gibbs free energy of intermediates for AEM and LOM of $Bi_2Ru_{34}O_{72}$, Bi-O_v-RuO_2 and RuO_2.

AEM			
Model / Intermediates	RuO_2	$Bi_2Ru_{34}O_{72}$	Bi-O_v-RuO_2
Slab	0	0	0
*OH	1.35	0.88	0.66
*O	2.21	2.42	2.21
*OOH	4.23	4.05	3.63
Slab+O_2	4.92	4.92	4.92

LOM			
Model / Intermediates	RuO_2	$Bi_2Ru_{34}O_{72}$	Bi-O_v-RuO_2
Slab	0	0	0
*OH	1.35	0.88	0.66
*O	2.21	2.42	2.21
*H	5.66	5.28	4.69
Slab+O_2	4.92	4.92	4.92

References

1. J. Rossmeisl, A. Logadottir and J. K. Nørskov, *Chemical Physics*, 2005, **319**, 178-184.

2. I. C. Man, H. Y. Su, F. Calle‐Vallejo, H. A. Hansen, J. I. Martínez, N. G. Inoglu, J. Kitchin, T. F. Jaramillo, J. K. Nørskov and J. Rossmeisl, *ChemCatChem*, 2011, **3**, 1159-1165.

3. S. Liu, Y. Chang, N. He, S. Zhu, L. Wang and X. Liu, *ACS Appl Mater Interfaces*, 2023, **15**, 20563-20570.

4. J. Abed, J. Heras-Domingo, R. Y. Sanspeur, M. Luo, W. Alnoush, D. M. Meira, H. Wang, J. Wang, J. Zhou, D. Zhou, K. Fatih, J. R. Kitchin, D. Higgins, Z. W. Ulissi and E. H. Sargent, *J Am Chem Soc*, 2024, **146**, 15740-15750.

5. J. He, X. Zhou, P. Xu and J. Sun, *Advanced Energy Materials*, 2021, **11**, 2102883.

6. N. Yao, H. Jia, J. Zhu, Z. Shi, H. Cong, J. Ge and W. Luo, *Chem*, 2023, **9**, 1882-1896.

7. Y. Qin, B. Cao, X.-Y. Zhou, Z. Xiao, H. Zhou, Z. Zhao, Y. Weng, J. Lv, Y. Liu, Y.-B. He, F. Kang, K. Li and T.-Y. Zhang, *Nano Energy*, 2023, **115**, 108727.

8. Q. Qin, T. Wang, Z. Li, G. Zhang, H. Jang, L. Hou, Y. Wang, M. Gyu Kim, S. Liu and X. Liu, *Journal of Energy Chemistry*, 2024, **88**, 94-102.

9. D. Chen, H. Zhao, R. Yu, K. Yu, J. Zhu, J. Jiao, X. Mu, J. Yu, J. Wu and S. Mu, *Energy & Environmental Science*, 2024, **17**, 1885-1893.

10. L. Deng, S. Liu, D. Liu, Y. M. Chang, L. Li, C. Li, Y. Sun, F. Hu, H. Y. Chen, H. Pan and S. Peng, *Small*, 2023, **19**, e2302238.

11. N. Li, L. Cai, C. Wang, Y. Lin, J. Huang, H. Sheng, H. Pan, W. Zhang, Q. Ji, H. Duan, W. Hu, W. Zhang, F. Hu, H. Tan, Z. Sun, B. Song, S. Jin and W. Yan, *J Am Chem Soc*, 2021, **143**, 18001-18009.

12. Z. Shi, J. Li, Y. Wang, S. Liu, J. Zhu, J. Yang, X. Wang, J. Ni, Z. Jiang, L. Zhang, Y. Wang, C. Liu, W. Xing and J. Ge, *Nat Commun*, 2023, **14**, 843.

13. Z. Fan, Y. Ji, Q. Shao, S. Geng, W. Zhu, Y. Liu, F. Liao, Z. Hu, Y.-C. Chang, C.-W. Pao, Y. Li, Z. Kang and M. Shao, *Joule*, 2021, **5**, 3221-3234.

14. X. Liu, S. Xi, H. Kim, A. Kumar, J. Lee, J. Wang, N. Q. Tran, T. Yang, X. Shao, M. Liang, M. G. Kim and H. Lee, *Nat Commun*, 2021, **12**, 5676.

15. H. Zhu, Y. Wang, Z. Jiang, B. Deng and Z.-J. Jiang, *Journal of Materials Chemistry A*, 2023, **11**, 25252-25261.

16. Y. Wang, Z. Li, L. Hou, Y. Wang, L. Zhang, T. Wang, H. Liu, S. Liu, Q. Qin and X. Liu, *ACS Applied Materials & Interfaces*, 2023, **15**, 14282-14290.

17. D. Chen, R. Yu, K. Yu, R. Lu, H. Zhao, J. Jiao, Y. Yao, J. Zhu, J. Wu and S. Mu, *Nat Commun*, 2024, **15**, 3928.

18. D. Wu, K. Kusada, S. Yoshioka, T. Yamamoto, T. Toriyama, S. Matsumura, Y. Chen, O. Seo, J. Kim, C. Song, S. Hiroi, O. Sakata, T. Ina, S. Kawaguchi, Y. Kubota, H. Kobayashi and H. Kitagawa, *Nat Commun*, 2021, **12**, 1145.

19. L. Li, G. Zhang, J. Xu, H. He, B. Wang, Z. Yang and S. Yang, *Advanced Functional Materials*, 2023, **33**.

20. D. Galyamin, J. Torrero, I. Rodriguez, M. J. Kolb, P. Ferrer, L. Pascual, M. A. Salam, D. Gianolio, V. Celorrio, M. Mokhtar, D. Garcia Sanchez, A. S. Gago, K. A. Friedrich, M. A. Pena, J. A. Alonso, F. Calle-Vallejo, M. Retuerto and S. Rojas, *Nat Commun*, 2023, **14**, 2010.

21. Y. Qin, T. Yu, S. Deng, X. Y. Zhou, D. Lin, Q. Zhang, Z. Jin, D. Zhang, Y. B. He, H. J. Qiu, L. He, F. Kang, K. Li and T. Y. Zhang, *Nat Commun*, 2022, **13**, 3784.

22. W. Zhu, F. Yao, K. Cheng, M. Zhao, C. J. Yang, C. L. Dong, Q. Hong, Q. Jiang, Z. Wang and H. Liang, *J Am Chem Soc*, 2023, **145**, 17995-18006.

23. M. Xiao, J. Liu, R. Li, Y. Sun, F. Liu, J. Gan and S. Gao, *Small*, 2024, **20**, e2400754.

24. Y. Chen, Y. Liu, L. Li, T. Sakthive, Z. Guo and Z. Dai, *Advanced Functional Materials*, 2024, DOI: 10.1002/adfm.202406587.

25. C. Lin, J.-L. Li, X. Li, S. Yang, W. Luo, Y. Zhang, S.-H. Kim, D.-H. Kim, S. S. Shinde, Y.-F. Li, Z.-P. Liu, Z. Jiang and J.-H. Lee, *Nature Catalysis*, 2021, **4**, 1012-1023.

26. H. Jin, S. Choi, G. J. Bang, T. Kwon, H. S. Kim, S. J. Lee, Y. Hong, D. W. Lee, H. S. Park, H. Baik, Y. Jung, S. J. Yoo and K. Lee, *Energy & Environmental Science*, 2022, **15**, 1119-1130.

27. F.-F. Zhang, C.-Q. Cheng, J.-Q. Wang, L. Shang, Y. Feng, Y. Zhang, J. Mao, Q.-J. Guo, Y.-M. Xie, C.-K. Dong, Y.-H. Cheng, H. Liu and X.-W. Du, *ACS Energy Letters*, 2021, DOI: 10.1021/acsenergylett.1c00283, 1588-1595.

28. Z. Y. Wu, F. Y. Chen, B. Li, S. W. Yu, Y. Z. Finfrock, D. M. Meira, Q. Q. Yan, P. Zhu, M. X. Chen, T. W. Song, Z. Yin, H. W. Liang, S. Zhang, G. Wang and H. Wang, *Nat Mater*, 2023, **22**, 100-108.

29. J. Shan, C. Ye, S. Chen, T. Sun, Y. Jiao, L. Liu, C. Zhu, L. Song, Y. Han, M. Jaroniec, Y. Zhu, Y. Zheng and S. Z. Qiao, *J Am Chem Soc*, 2021, **143**, 5201-5211.